Available online at www.sciencedirect.com
ScienceDirect
Journal of Nuclear Materials 373 (2008) 378–386
journal of nuclear materials
www.elsevier.com/locate/jnucmat

Structural behavior of β-thorium phosphate diphosphate (β-TPD) irradiated with ion beams

C. Tamain [a], F. Garrido [b,*], L. Thomé [b], N. Dacheux [a], A. Özgümüs [a]

[a] Groupe de Radiochimie, Institut de Physique Nucléaire, CNRS-IN2P3-Univ. Paris-Sud 11, Bâtiment 100, F-91406 Orsay Campus, France
[b] Centre de Spectrométrie Nucléaire et de Spectrométrie de Masse, CNRS-IN2P3-Univ. Paris-Sud, Bâtiment 108, F-91405 Orsay Campus, France

Received 21 December 2006; accepted 26 June 2007

Abstract

β-thorium phosphate diphosphate ceramic (β-TPD), β-$Th_4(PO_4)_4P_2O_7$, was proposed as a potential actinide-bearing phase for nuclear waste storage. Self-irradiation by α-decays, due to the actinide loading, could affect the good intrinsic performances of this material. The evaluation of irradiation effects on the chemical durability of the ceramic is a crucial issue. Radiation effects were simulated by external ion beam irradiations. Under high-energy ion irradiation, amorphization was achieved above a critical threshold for electronic energy loss ($S_e = 5$ MeV μm^{-1}). Thermal annealing enables to fully recover the initial crystalline structure after heating for 15 h above 973 K. Amorphization appears thus completely reversible. The activation energy of annealing is equal to 2.8 eV. Ion beam induced amorphization and recrystallization by thermal annealing were found to be isotropic processes. Irradiations in the nuclear stopping regime lead to a complete amorphization of β-TPD at a critical dose of 0.2 dpa.

1. Introduction

In France, one of the likely options foreseen for the nuclear waste issue consists of the long-term immobilization of minor actinides and long half-life fission products in the field of an underground repository [1]. Ceramics, especially phosphate based ones, were clearly identified as good candidates for the immobilization of long half-life radionucleides [2,3]. Among them, thorium phosphate diphosphate (β-TPD), β-$Th_4(PO_4)_4P_2O_7$, has been proposed as an actinide-bearing phase of immobilization in the field of the nuclear waste management. This material, which can be loaded *in situ* with large amounts of tetravalent actinides [4,5], appears to be highly resistant to aqueous corrosion [6,7] and exhibits a high thermal stability.

However, in the field of such an application, this material must be resistant to radiation damage. Actually, it will be subjected to α-decay of incorporated actinide elements, which produce typically 5-MeV α-particles and heavy recoil nuclei of about 100 keV. The kinetic energy of produced particles can be transferred either to electrons by ionization and electronic excitations or to atoms through ballistic processes involving elastic collisions. In an α-decay, the nuclear contribution predominates for low-energy recoil nuclei (∼100 keV), while the transfer is mainly electronic for the medium-energy α-particle (∼5 MeV). It is well known that ion irradiation can deeply modify the crystalline structure and consequently the physical and chemical properties of a material [8]. Indeed, radiation can induce the transformation of the crystalline phase into an amorphous one. Many studies have been previously devoted to the amorphization trend of phosphate-based ceramics. Karioris et al. [9] irradiated monazite ($LnPO_4$) with 3-MeV Kr at room temperature and evidenced that this material amorphizes at a fluence smaller than 5×10^{14} cm^{-2}. According to Meldrum et al. phosphate-based ceramics exhibit a lower sensibility to ion-beam irradiation than silicate analogues [10]. The

* Corresponding author. Tel.: +33 1 69 15 52 57.
E-mail address: Frederico.Garrido@csnsm.in2p3.fr (F. Garrido).

0022-3115/$ - see front matter © 2007 Elsevier B.V. All rights reserved.
doi:10.1016/j.jnucmat.2007.06.017

critical dose of amorphization in monazite was estimated to be 0.4 dpa (displacement per atom) [11]. In the case of britholite ceramic containing one silicate group (i.e. $Ca_9Nd(SiO_4)(PO_4)_5F_2$), the critical amorphization dose was estimated to be in the range of 0.20–0.45 dpa [11]. Some studies revealed that the amorphization occurs at a lower critical dose when the amount of silicates groups per unit formula is increased [12]. This observation is linked to an increased capability of annealing under α irradiation when the rate of phosphate groups increases.

The present work deals with the study of consequences of irradiation on the structure of the β-TPD ceramic through the production of radiation defects in a storage matrix in both electronic and nuclear regimes. In this context, samples were irradiated with ion beams at various energies (i.e. 840-MeV Kr, 390-MeV Xe, 95-MeV I, 410-MeV S, 1.6-MeV He, 4-MeV Au) in order to perform a systematic study of the influence of both electronic and nuclear stoppings. It is worth noting that, in order to alter a significant thickness of the material, the range of energy used in these experiments was chosen far from the conditions existing in a real nuclear waste storage. Moreover the ion flux used during external ion irradiation is by several orders of magnitude larger than the dose rate expected in nuclear wastes. In spite of these limitations, this approach allows us to study the behavior of such ceramics under irradiation performed in extreme conditions. The structural evolution of the materials was mainly followed by X-ray diffraction (XRD) analyses, and completed by complementary techniques, such as scanning electron microscopy (SEM), electron probe microanalyses (EPMA) and μ-Raman spectroscopy. In a second part, thermal annealing experiments are described. Experiments were performed either on β-TPD or on β-TUPD solid solutions (β-$Th_{4-x}U_x(PO_4)_4P_2O_7$) to investigate the influence of the substitution of thorium by other tetravalent actinide on the resistance of the material to irradiation.

2. Experimental procedures

2.1. Preparation of the samples

β-TPD samples were prepared by wet chemistry route [4,13] based on the initial precipitation of thorium phosphate hydrogen phosphate hydrate (TPHPH), $Th_2(PO_4)_2(HPO_4)\cdot H_2O$, as a crystallized precursor [14,15]. β-TUPD samples were synthesized through the same method, i.e. by precipitation of TUPHPH solid solutions: $Th_{2-x/2}U_{x/2}(PO_4)_2(HPO_4)\cdot H_2O$. In both cases, concentrated thorium chloride (and eventually uranium chloride) and phosphoric acid solutions (respectively of 5×10^{-4} mol g^{-1} i.e. 0.7 M and 4×10^{-3} mol g^{-1} i.e. 5 M) were mixed, considering a mole ratio $r = PO_4/Th$ (or $PO_4/(Th+U)) = 3/2$, then slowly evaporated at 150 °C for 8–10 days in PTFE (polytetrafluoroethylene) containers. For TUPHPH solid solutions, the mole ratio Th/U was fixed to 1/9 (i.e. 10 wt% (U) in the solid, to prepare $Th_{1.8}U_{0.2}(PO_4)_2(HPO_4)\cdot H_2O$ solid solution).

The crystallized samples were separated from the supernatant by centrifugation at 4000 rpm. They were washed several times with deionized water then with ethanol and finally dried at 90 °C for 2–3 h. The obtained TPHPH powder was extensively characterized through XRD, EPMA and SEM experiments. The surface area was estimated at 15 m^2 g^{-1} from the B.E.T. method (N_2 adsorption). All the results match well with the data obtained in a previous study and are in good agreement with the preparation of single phase precursors [14,13].

After heating at 450 °C (in air for TPHPH or under inert atmosphere for TUPHPH to avoid any oxidation of tetravalent uranium), the obtained powder was sintered *via* a room temperature uniaxial pressing at 250 MPa in a 10 mm diameter cylindrical die [16]. The resulting pellets were then thermally heated in alumina boats for 15 h at 1200–1250 °C to prepare β-TPD and β-TUPD as described in literature [17]. This sintering step enables to increase the cohesion between the grains in the solid and leads to a compound with an enhanced mechanical resistance. The resulting pellets obtained are cylinders of about 1 mm in thickness and 9 mm in diameter with a density ranging from 94% to 99% of the value calculated from X-ray diffraction data.

2.2. Irradiations experiments

Irradiations were performed at room temperature on sintered pellets using several ion beams: 840-MeV Kr and 410-MeV S ions at the GANIL accelerator (Caen), 450-MeV Xe ions at the ISL cyclotron (Berlin), 170-MeV I ions using the Tandem (Orsay), 4-MeV Au and 1.6-MeV He ions using the Aramis facility (Orsay). The projected ion range as well as the electronic (S_e) and nuclear (S_n) contributions to the stopping power were determined with the Monte Carlo simulation code SRIM 2006 [18] assuming the genuine target density of the pellet (theoretical density is 5.19 g cm^{-3}) [4] and a displacement energy threshold of 25 eV for all atoms [19]. These values as well as the thickness through which the stopping powers are constant (with an accuracy of 10%) are gathered in Table 1. In the case of 410-MeV S and 170-MeV I irradiations, samples were wrapped into an aluminum sheet in order to avoid a radioactive contamination of the experimental box. Consequently, ions loose a part of their energy in the aluminum foil before interacting with the solid leading to an effective energy of the ion at the surface of about 390-MeV for S ions and 95-MeV for I ions. According to the values of stopping power (see Table 1), it can be anticipated that irradiation-induced defects are mainly created through electronic excitation for Kr, Xe, I and S ions. The nuclear contribution is indeed lower by more than two orders of magnitude than the electronic contribution in these conditions. On the contrary, nuclear and electronic contributions are similar for Au irradiations.

Table 1
Electronic and nuclear stopping powers (S_e and S_n) for the different irradiation experiments

Ion	Incident energy (MeV)	Range (μm)	Stopping power (MeV μm^{-1})			
			Electronic S_e		Nuclear S_n	
			Surface	$\Delta d_{constant}$ (μm)	Surface	$\Delta d_{constant}$ (μm)
Au	4	0.8	2.6	≈0.2	2.5	≈0.4
Xe	450	29	21.4	≈13	4.1×10^{-2}	≈2.5
I	170[a]	11	15.4	≈2	9.8×10^{-2}	≈1.5
Kr	840	70	10.4	≈20	7×10^{-3}	≈9
S	410[a]	110	2.5	≈10	1.3×10^{-3}	≈25
He	1.6	4.2	0.4	≈1	4×10^{-4}	≈0.5

Thickness over which the stopping power is constant with an accuracy of 10%.
$\Delta d_{constant}$ corresponds to the thickness in which the stopping power is constant with an accuracy of 10%.
[a] Samples were wrapped into aluminium sheet of 11.5 μm (410-MeV S) and 5 μm (170-MeV I) of thickness to avoid the contamination of the experimental box. The effective energy at the surface of the sample is 390 MeV and 95 MeV, respectively.

2.3. Characterization

Each irradiated sintered sample was characterized through XRD. The diagrams were collected with a Brücker D8 Advanced Roentgen diffractometer system using CuK$_\alpha$ rays ($\lambda = 0.15418$ nm). The amorphous fraction f_A of irradiated samples, which gives the relative ratios of amorphous and crystalline phases, was evaluated from the net areas of the corresponding XRD lines by using the following formula [20]:

$$f_A = 1 - \frac{\sum_{i=1}^{x} \frac{A_i^{\text{irradiated}}}{A_i^{\text{unirradiated}}}}{x}, \quad (1)$$

where $A_i^{\text{irradiated}}$ and $A_j^{\text{unirradiated}}$ represent the net area of the ith XRD line in the diagram recorded on the irradiated and unirradiated sample, respectively, and x denotes the number of lines considered. As the maximum X-ray penetration in β-TPD is 9 μm, the characterization by XRD analysis only concerned the irradiated layer for high-energy ion irradiation (i.e. Xe, Kr, S, I ions in our experimental conditions). XRD diagrams were collected using the grazing mode for Au-irradiated samples in order to probe the irradiated zone only.

Samples were characterized by EPMA using a Cameca SX 50 apparatus (acceleration voltage of 15 kV and current of 10 nA). The calibration standards were $SmPO_4$ (K_α ray of phosphorous), ThO_2 (M_α ray of thorium) and UO_2 (M_β ray of uranium). The counting time was fixed to 10–30 s for a spot size of 1 μm. These experiments enabled us to check the homogeneity, the purity and the chemical composition of the sintered samples before and after irradiation.

SEM analyses were collected using a Hitachi S2500 scanning electron microscope.

μ-Raman spectra were recorded by the means of a Dilor–Jobin Yvon apparatus using an argon laser working at 514.5 nm. The power varied from 50 to 100 mW and the laser beam was focused on the sample with an Olympus microscope.

ESR spectra were recorded with a Brucker spectrometer operating at X-band (9.5 GHz). The first derivative of the electron paramagnetic resonance absorption was obtained versus the magnetic field.

2.4. Annealing experiments

Annealing experiments of fully amorphized β-TPD pellets were performed in alumina boats using Pyrox HM 40 or Adamel FR 20 furnaces. Samples were heated in air at temperature ranging from 473 K to 1173 K. After a heating step completion ESR spectra and XRD diagrams were recorded to study the structural recovery.

3. Results and discussion

3.1. Structural consequences of irradiation

The first class of irradiations aimed at studying the influence of the electronic stopping power on the structural stability of the material by using high-energy ion beams (840-MeV Kr, 450-MeV Xe, 95-MeV I, 390-MeV S, 1.6-MeV He). XRD analyses performed on irradiated samples illustrate the structural evolution of the crystal structure during irradiation (Fig. 1). The increase of the Full Width at Half Maximum (FWHM) and the simultaneous decrease of the net area of the XRD lines clearly evidence the progressive amorphization of the material. This amorphization is completed (leading to an amorphous fraction $f_A = 1$) above a critical fluence in the case of high electronic stopping power irradiations ($S_e = 10.4$ MeV μm^{-1}, 15.4 MeV μm^{-1} and 21.4 MeV μm^{-1} for 840-MeV Kr, 95-MeV I and 450-MeV Xe, respectively). *In situ* XRD experiments at the CHEXPIR facility (GANIL) performed on samples irradiated with 840-MeV Kr ions revealed that the variation of the amorphous fraction versus ion fluence can be accurately fitted with the direct impact model [21,22]:

$$f_A = 1 - \exp(-\sigma_a \Phi), \quad (2)$$

where f_A represents the amorphous fraction of the material subjected to irradiation, Φ is the ion fluence and σ_a is the cross-section of the cylinder around the ion path in which the material is amorphized. In the case of 840-MeV Kr

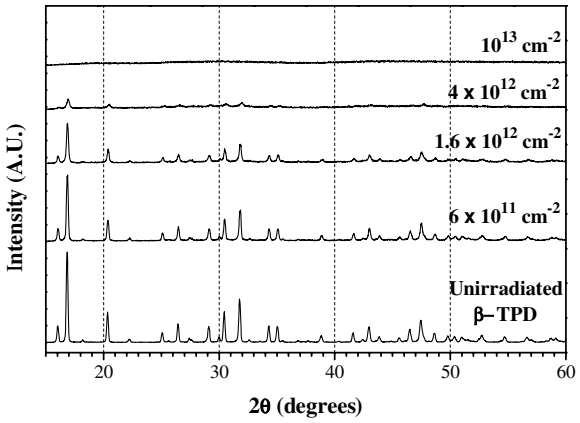

Fig. 1. XRD diagrams of sintered pellets of β-TPD irradiated at different fluences (840-MeV Kr).

irradiation, this fit allowed to extract the cross-section for the radiation damage formation, i.e. $\sigma_a = (5.0 \pm 0.7) \times 10^{-13}\,cm^2$, which corresponds to a track diameter of 8.0 ± 0.5 nm.

It was also shown that the amorphization was isotropic. Indeed, the three unit cell parameters decrease similarly (about 1%), leading to a relative compaction of the unit cell volume of about 3% when the amorphization is complete [22]. Such a densification induced by irradiation is likely to be due to the low atomic density of crystalline TPD. Thus phosphate groups, remaining intact even after complete amorphization of the material, can be more efficiently packed in the amorphous phase.

The macroscopic observation of the complete amorphization by XRD was completed by SEM observations of samples irradiated with 450-MeV Xe ions (Fig. 2). During these irradiation steps, half of the sample surface was hidden by a mask so that only the other half part was irradiated. The corresponding part was thus amorphized as confirmed from XRD analyses. Some micrographs recorded on the borderline between both zones (Fig. 2(a) and Fig. 2(b)) evidenced an obvious influence of the amorphization on the microstructure of the material, especially in the field of the occurrence of grain boundaries and of the residual porosity. This phenomenon which could suggest a 'vitrification' step, is observed at the surface and over the whole thickness of the irradiated domain (Fig. 2(c)), i.e. 30 μm in these experimental conditions.

Irradiation experiments at a lower value of the electronic stopping power were also performed (with $S_e = 2.5\,MeV\,\mu m^{-1}$ and $0.4\,MeV\,\mu m^{-1}$ for 410-MeV S and 1.6-MeV He, respectively). In the case of irradiations with 410-MeV S, XRD analyses revealed that the sample is only partially amorphized: the amorphous fraction reaches a plateau which value is inferior to 1 (Fig. 3). SEM observations of the thickness of irradiated sample (410-MeV S at a fluence $5 \times 10^{13}\,cm^{-2}$) reveals heterogeneities in the microstructure with a disappearing of the grain boundaries between 70 and 110 μm along the ion range (Fig. 4). This 'vitrification' phenomenon, which is similar to that

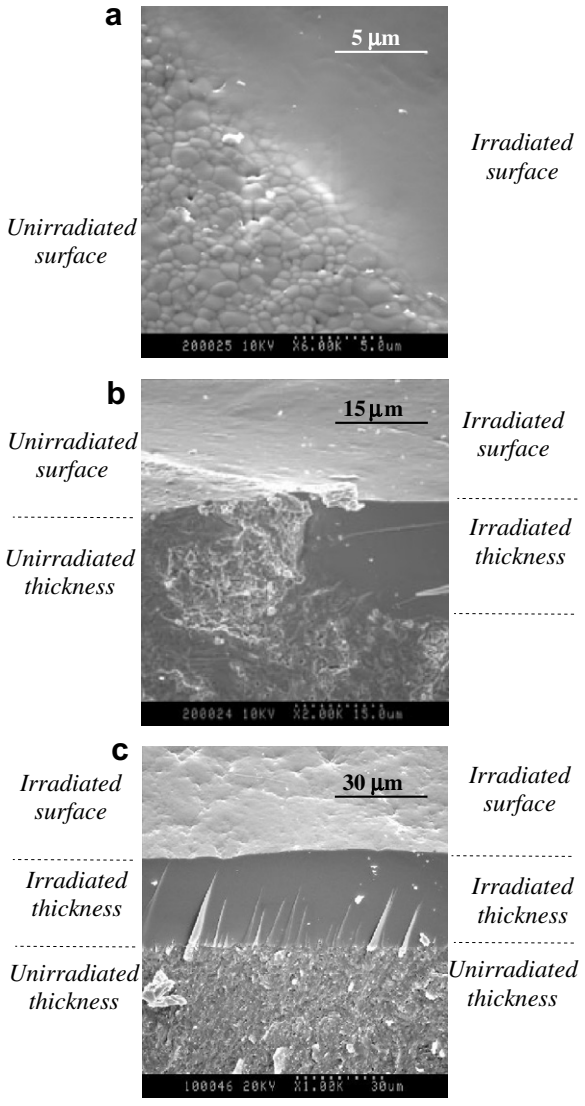

Fig. 2. SEM observations of β-TPD irradiated sample on the half part of its surface (450-MeV Xe, $2 \times 10^{14}\,cm^{-2}$).

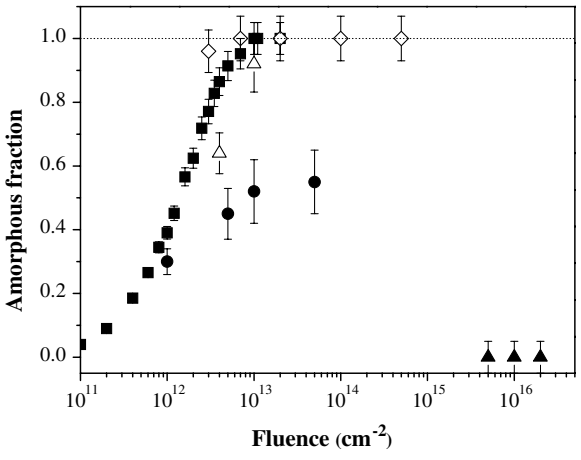

Fig. 3. Variation of the amorphous fraction f_A versus the ion fluence for the different irradiation experiments on β-TPD (■: 840-MeV Kr; △: 170-MeV I; ◇: 450-MeV Xe; ●: 410-MeV S; ▲:1.6-MeV He).

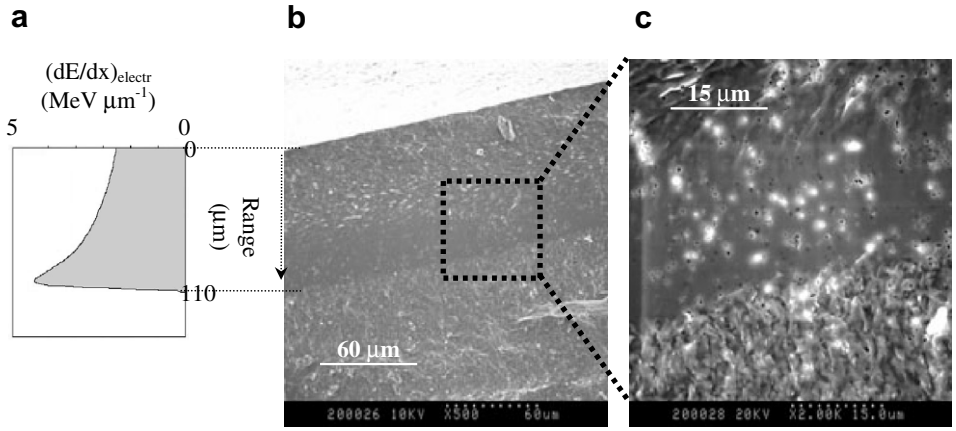

Fig. 4. Variation of the electronic stopping versus ion penetration depth (a). SEM observations of β-TPD irradiated sample (410-MeV S, 5×10^{13} cm^{-2}) (b, c).

previously described (Fig. 2), occurs at some depth along the ion path and abruptly ends at the end of the trajectory. This profile reminds the variation of the electronic stopping power along the ion range in the ceramic (Fig. 4). Thus, it appears that the 'vitrification' zone (corresponding to the amorphised region of the sample) corresponds to the localization of the maximum of electronic stopping power, the so-called 'Bragg peak' (around 5 MeV µm^{-1} in the present case according to SRIM calculations). Thus the apparent partial amorphization of the material even at high fluence (10^{14} cm^{-2}) should be interpreted as the result of the overlapping of the presence of amorphous and undamaged regions explored by XRD. From this observation it can be concluded that the complete amorphization of the material occurs above a critical threshold in electronic stopping power ($S_e = 5$ MeV µm^{-1}).

The experiments enable us to determine the behavior of β-TPD under irradiation in the electronic stopping regime. Two extreme behaviors were thus evidenced:

(1) complete amorphization above a critical fluence (around 10^{13} cm^{-2}) when the stopping power is higher than 5 MeV µm^{-1}.
(2) absence of amorphization (on the basis of the XRD characterization) for electronic stopping power values inferior to 2 MeV µm^{-1} (such as 1.6-MeV He, $S_e = 0.4$ MeV µm^{-1}).

The influence of the nuclear stopping power contribution was also investigated. In this aim, irradiation experiments were driven with 4-MeV Au for which the electronic and nuclear contributions of the stopping power are almost the same (Table 1). Indeed, irradiation experiments with 410-MeV S and 4-MeV Au exhibit identical S_e values, but differ by their S_n values. Thus, the comparison between both kinds of experiments shows directly the influence of the nuclear stopping power on the structural consequences of irradiation. SEM analyses revealed a significant modification of the microstructure of the surface of irradiated zones under 4-MeV Au ion beam (Fig. 5) with a disappearing of the grain boundaries under irradiation. The variation of the amorphous fraction (determined from grazing XRD) is presented in Fig. 6. Amorphization is completed at a fluence of 5×10^{13} cm^{-2} which corresponds to a critical dose of 0.2 dpa. This value is consistent with those obtained in previous works [23,24].

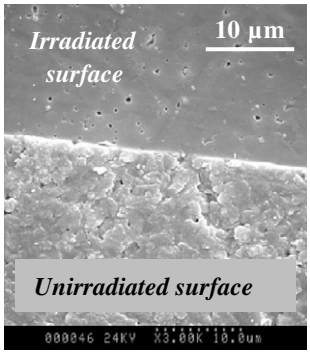

Fig. 5. SEM observation of β-TPD irradiated with 4-MeV Au, 5×10^{14} cm^{-2}.

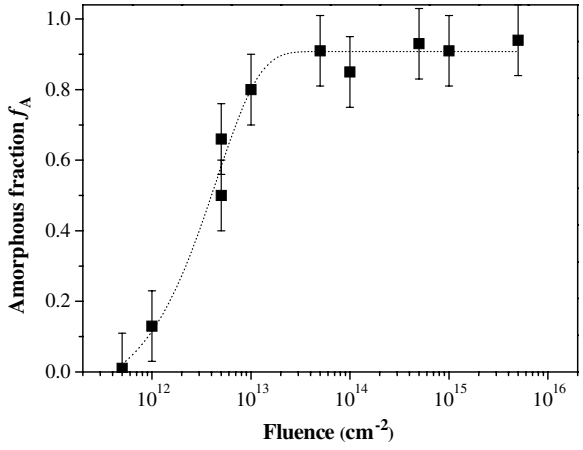

Fig. 6. Variation of the amorphous fraction f_A versus ion fluence during the irradiation of β-TPD with 4-MeV Au.

Table 2
Electron probe micro analyses (EPMA) results for β-TPD and β-TUPD samples before and after irradiation

	β-TPD		β-TUPD		
	Unirradiated	Xe 2×10^{14} cm^{-2}	Unirradiated	S 5×10^{13} cm^{-2}	I 4.25×10^{12} cm^{-2}
O (wt%)	24.8 ± 0.3	25.1 ± 0.1	24.9 ± 0.8	25.3 ± 0.2	25.1 ± 0.2
P (wt%)	12.6 ± 0.2	12.7 ± 0.1	12.5 ± 0.5	12.9 ± 0.1	12.7 ± 0.1
Th (wt%)	61.2 ± 0.6	62.8 ± 0.5	56.8 ± 1.1	58.0 ± 0.9	58.4 ± 0.9
U (wt%)	–	–	5.1 ± 0.5	5.1 ± 0.4	5.0 ± 0.3
Mole ratio (Th + U)/P	0.65 ± 0.02	0.66 ± 0.01	0.66 ± 0.02	0.65 ± 0.02	0.66 ± 0.01
Mole ratio U/(Th + U)	–	–	0.80 ± 0.09	0.79 ± 0.09	0.77 ± 0.09

All the previously described experiments were performed simultaneously on β-TPD and β-TUPD samples with various substitution rates (10 and 40 uranium mol%). The behavior of such materials under irradiation appears quite similar which evidences that the substitution of thorium by tetravalent uranium induces no significant influence on the behavior of the ceramic under irradiation.

3.2. Chemical consequences of irradiation

The irradiated samples were submitted to physico-chemical characterization experiments in order to investigate the influence of irradiation on the chemical composition of β-TPD and associated β-TUPD solid solutions.

EPMA were driven on unirradiated and irradiated samples to show the influence of irradiation on the elemental composition (Table 2). In both cases, irradiation does not modify the elemental composition. Indeed, for β-TPD and β-TUPD samples, respectively, the Th/P and (Th + U)/P mole ratios remain equal to 2/3 after irradiation, which appears in good agreement with that expected on the basis of the β-TPD (or β-TUPD) chemical formula. Furthermore, in the presence of uranium, irradiation may induce a local oxidation for this element. The constancy of the U/(Th + U) mole ratio and of elementary weight percents shows that there is no significant change in the uranium oxidation state in the irradiated zone.

Complementary characterizations through μ-Raman spectroscopy were developed in order to examine the nature of the chemical bonds in irradiated and unirradiated samples (Fig. 7). The spectrum of the irradiated sample presents an important baseline due to the strong luminescence induced by the irradiation defects excited by the laser source. Except from this baseline, both spectra of unirradiated and irradiated samples appear similar and exhibit all the vibration bands characteristic of phosphate and diphosphate groups in β-TPD (Table 3). Vibration bands belonging to the P–O bond of the PO_4 groups can be assigned considering the data reported in the literature [14]: δ_s (372, 428 cm^{-1}), δ_{as} (574, 619 cm^{-1}), ν_S (990 cm^{-1}) and ν_{as} (1023, 1150 cm^{-1}). The vibration band located between 720 and 760 cm^{-1} corresponds to the symmetric stretching mode of the P–O–P bridge and confirms the presence of diphosphate groups in the irradiated sample. Thus, phosphate tetrahedra and P–O–P bridges are not altered during irradiation. They may be rearranged without destruction during the amorphization process. This phenomenon was previously reported in literature for silica which exhibits a densification under irradiation, due to the shift of the SiO_4 tetrahedral groups from their initial crystallographic positions [25]. This explanation of rearrangement is also consistent with the decrease of the cell volume observed from XRD study.

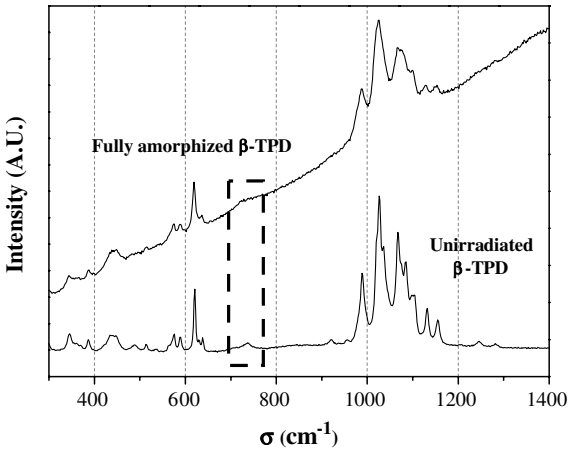

Fig. 7. μ-Raman spectrum of unirradiated and irradiated β-TUPD samples samples (840-MeV Kr, 10^{13} cm^{-2}).

Table 3
Attribution of μ-Raman bands (cm^{-1}) for virgin and irradiated β-TPD at several Kr fluences

	P–O vibrations				P–O–P vibrations	
	δ_s (cm^{-1})	δ_{as} (cm^{-1})	ν_s (cm^{-1})	ν_{as} (cm^{-1})	ν_s (cm^{-1})	ν_{as} (cm^{-1})
Unirradiated β-TPD	350–450	490–645	960	970–1190	700–740	920–950
10^{12} cm^{-2}	350–450	490–650	950	970–1180	700–740	910–970
7×10^{12} cm^{-2}	310–480	490–660	N.O.	970–1200	680–800	N.O.
2×10^{13} cm^{-2}	320–500	450–650	N.O.	900–1220	680–820	N.O.

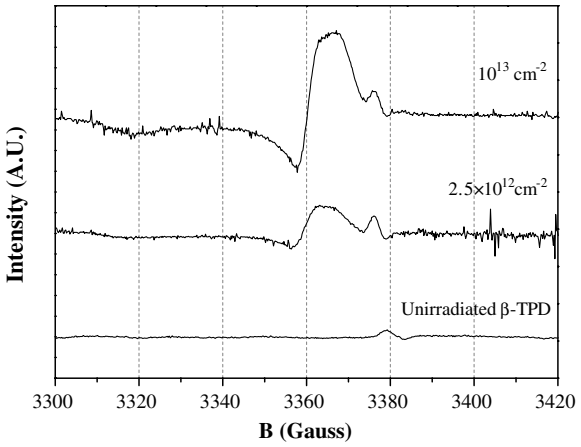

Fig. 8. ESR spectra of unirradiated and irradiated β-TUPD samples for several fluences samples (840-MeV Kr).

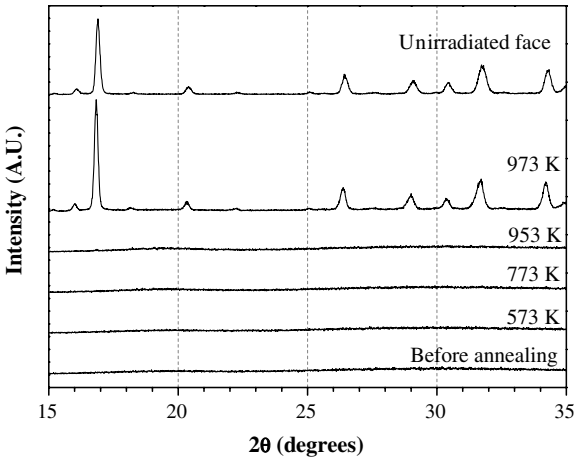

Fig. 9. Variation of XRD diagrams of amorphized β-TPD (840-MeV Kr) during isochronal annealing (10 h-step) for several heating temperatures.

The comparison between the behavior of the material under irradiation as seen by XRD and μ-Raman spectroscopy deserves some discussion. Classical diffraction techniques provide information averaged over many unit cells and therefore information on the long-range order. Conversely, Raman spectroscopy involves the scattering of radiation by specific molecular bonds and gives us a useful method to investigate the material at a more local scale. Thus, observations performed with both techniques lead to the hypothesis of a two levels of disorder induced by irradiation. Although the long-range order is destroyed by ion irradiation, the covalent chemical bonds remain unaltered even above the 'critical fluence' of amorphization.

ESR analyses were also performed on the samples irradiated with predominant electronic interactions (Fig. 8) in order to evidence the presence of paramagnetic defects. The large band observed around 3360 Gauss, which intensity increases with the irradiation fluence, probably corresponds to the POO$^{\bullet}$ radical with the single electron localized on the terminal oxygen [24]. This group may originate in the displacement of an oxygen atom of a phosphate group to a P–O bond.

3.3. Thermal annealing

The capability of amorphized samples to recover the initial crystal structure by thermal annealing was also examined. In this aim, isochronal and isothermal experiments were performed on fully amorphized samples.

Isochronal experiments consisted of heating fully amorphized samples for 10 h-steps at given temperatures between 473 and 973 K. The samples were characterized through XRD after each step (Fig. 9). As it is observed in this figure, the crystal structure is fully recovered above 973 K.

ESR analyses were also performed on the annealed samples after each 10 h-step. The paramagnetic defects observed for irradiated samples progressively disappear at 473 K and vanished completely at 773 K (Fig. 10). It is worth mentioning that at the same temperature the crystal-

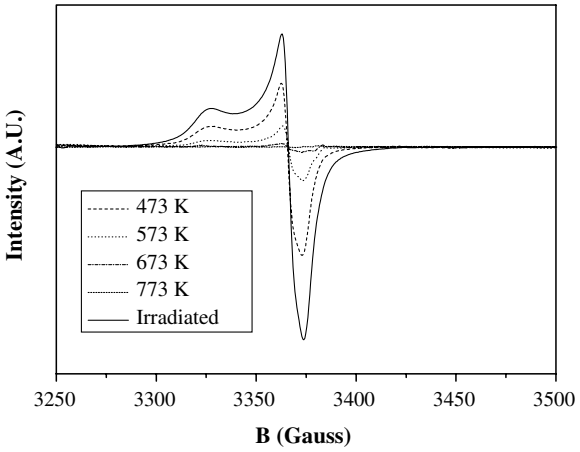

Fig. 10. Variation of ESR spectra of fully amorphized β-TPD (840-MeV Kr) during isochronal annealing (10 h-step) for several heating temperatures.

line structure as seen by XRD is amorphous. This observation reveals two stages of annealing similar to the two alteration levels under irradiation previously discussed: point and extended defects created in the phosphate sublattice are annealed before the global recrystallization of the structure.

Isothermal experiments were then realized at 1023 K or 1173 K to get a rapid annealing in a few hours; the last one being performed at 873 K. After each annealing step (1 h), XRD diagrams were recorded and the evolution of the amorphous fraction was evaluated from Eq. (1) (Fig. 11(a)). The kinetics of annealing was studied using the Johnson–Mehl–Avrami–Kolmogorov (JMAK) formalism [26,27], i.e. using the following equation:

$$f_A = \exp(-(kt)^n), \tag{3}$$

where t corresponds to the annealing time (s), k is the kinetic constant (s^{-1}) and n the JMAK coefficient which value depends on the grow-up process of the crystalline germs.

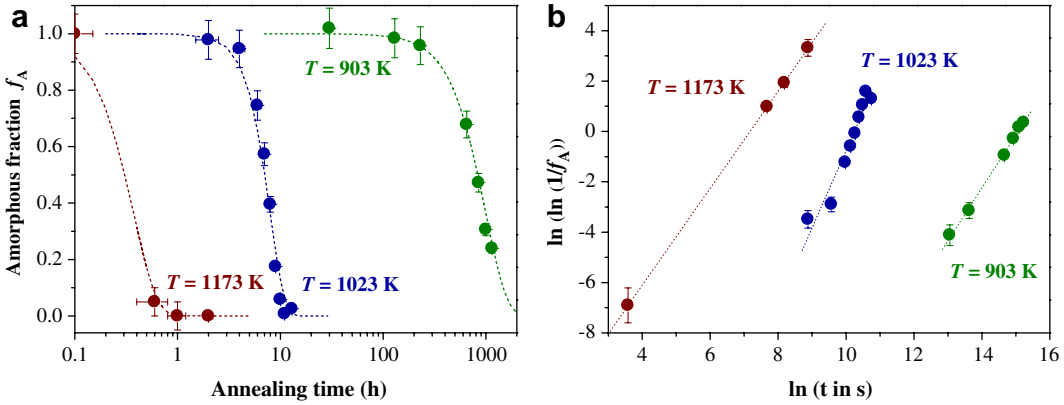

Fig. 11. Evolution of the amorphous fraction f_A of initially fully amorphized β-TPD during the annealing for several temperatures (a). Representation of $\ln(\ln(1/f_A)$ versus $\ln(t)$ (John–Mehl–Avram–Kolmogorov formalism) (b).

Table 4
John–Mehl–Avrami–Kolmogorov coefficients (k and n) for different temperatures of annealing

T (K)	903	1023	1173
n	2.1 ± 0.1	3.1 ± 0.4	1.9 ± 0.1
k (s^{-1})	$(2.8 \pm 1.0) \times 10^{-7}$	$(3.5 \pm 1.6) \times 10^{-5}$	$(7.5 \pm 1.2) \times 10^{-4}$

This equation can be developed in a linear expression:

$$\ln\left(\ln\left(\frac{1}{f_A}\right)\right) = n\ln(t) + n\ln(k). \quad (4)$$

The n and k values were thus estimated from linear regression of the experimental data (Fig. 11(b) and Table 4). Since the n values are found between 2 and 3, the annealing process is expected to occur mainly by nucleation [26].

The evolution of the unit cell parameters was followed during the annealing at 1023 K. A relative increase of 1% is observed for each unit cell parameter a, b and c (i.e. 3% for the unit cell volume) (Fig. 12). The relative increase by annealing appears symmetric to the relative decrease observed under irradiation which indicates that the structural alteration under irradiation is reversible thanks to the thermal annealing. Moreover, this annealing process, like the damage creation, is isotropic, in accordance with the nucleation process proposed.

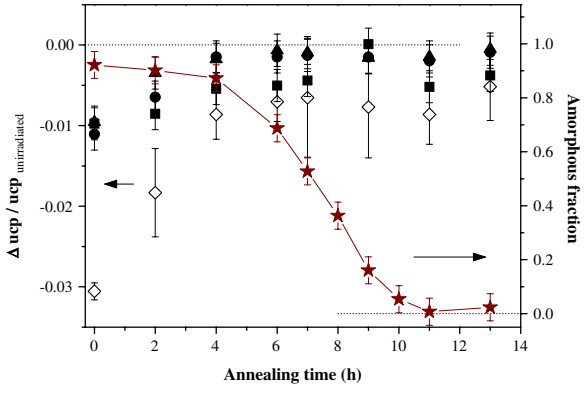

Fig. 12. Evolution of the unit cell parameters (ucp) and of the amorphous fraction during the isotherm annealing of β-TPD ($T = 1023$ K): ●: a; ▲: b; ■: c; ◇: V; ★: f_A.

On the basis of the kinetic constants values determined from the JMAK formalism at these temperatures, the activation energy of annealing was evaluated from the Arrhenius law (Table 4):

$$k = F_0 \exp\left(\frac{-E_A}{RT}\right), \quad (5)$$

where E_A is the activation energy of annealing and F_0 is the jump frequency. The activation energy value was found to be equal to 2.8 ± 0.1 eV (i.e. 270 ± 10 kJ mol^{-1}) from the linear regression obtained when plotting the variation of $\ln(k)$ versus the reciprocal of temperature. This value appears similar to that reported for the monazite $LnPO_4$ matrix, estimated to be 2.7–2.8 eV (i.e. 260–270 kJ mol^{-1}) studied with the same objective [11].

4. Conclusion

Irradiation experiments performed on β-TPD under ion beams at room temperature induce significant structural modifications. The complete amorphization can be reached when the deposited energy loss is sufficient provided a critical fluence (which depends on stopping power) is exceeded. The behavior of the ceramic was determined versus the electronic stopping power. Above 5 MeV μm^{-1}, β-TPD fully amorphizes for fluence higher than 10^{13} cm^{-2} while below 1 MeV μm^{-1}, no amorphization is observed. Concerning nuclear stopping, the critical dose for amorphisation was estimated to be 0.2 dpa.

In both cases, the microstructure of the material is deeply modified, with a disappearing of the grain boundaries. The structural alteration is isotropic with associated unit cell volume drop of about 3%, probably due to the shift of the phosphate groups. On the contrary, the chemical structure is not modified since the elemental composition of β-TPD (and associated β-TUPD solid solutions) remains unchanged after irradiation. Besides, μ-Raman

analyses revealed that phosphate bounds are kept largely intact even in the fully amorphized material. This observation leads to propose two levels in the structural alteration of the material under irradiation. The first one, evaluated from the amorphous fraction, is associated to the crystalline structure. The second one corresponds to the phosphate sublattice where inter chemical bounds are not completely altered during irradiation.

Annealing capability of β-TPD, which enables to recover its initial crystalline structure for an amorphized sample, was also evidenced. The associated activation energy of annealing is about 2.8 eV (i.e. 270 kJ mol^{-1}). The structural recovering occurs in two steps: the first one concerns the crystalline structure and can be followed by monitoring the amorphous fraction in the material. It appears to be isotropic and mainly occurs by nucleation. The second one can be associated to the phosphate sublattice where local defects are annealed before the crystalline structure is restored.

The effect of this structural alteration of β-TPD due to irradiation on several physico-chemical properties such as the resistance of the material to aqueous alteration (chemical durability) was also studied. The results of the irradiation/leaching couplings combining a dual approach based on the kinetics and thermodynamics of the dissolution was developed [28–30].

Acknowledgements

This work was financially and scientifically supported by the French research program NOMADE (GDR 2023 CEA/CNRS/COGEMA) and by the ACTINET network (JRP 02-28). The authors are grateful to the GANIL, ISL, Tandem and ARAMIS staffs for their help during the irradiation experiments. The authors also want to thank Renaud Podor, Johan Ravaux and Alain Kolher from LCSM (Université Henri Poincaré Nancy-I, France) for performing EPMA and SEM observations and Thérèse Lhomme from CREGU (Université Henri Poincaré Nancy-I, France) for her extensive help during the characterization of the samples by μ-Raman.

References

[1] J.C. André, C.R. Acad. Sci. Paris – II A 333 (2001) 835.
[2] V. Brandel, N. Dacheux, M. Genet, J. Solid State Chem. 121 (1996) 467.
[3] N. Dacheux, N. Clavier, A.C. Robisson, O. Terra, F. Audubert, J.E. Lartigue, C. Guy, C.R. Chim. 7 (2004) 11414.
[4] P. Benard, V. Brandel, N. Dacheux, S. Jaulmes, S. Launay, C. Lindecker, M. Genet, D. Louër, M. Quarton, Chem. Mater. 8 (1996) 181.
[5] N. Dacheux, A.C. Thomas, V. Brandel, M. Genet, J. Nucl. Mater. 257 (1998) 108.
[6] A.C. Thomas, N. Dacheux, P. Le Coustumer, V. Brandel, M. Genet, J. Nucl. Mater. 281 (2000) 91.
[7] A.C. Thomas, N. Dacheux, P. Le Coustumer, V. Brandel, M. Genet, J. Nucl. Mater. 295 (2001) 249.
[8] W.J. Weber, R.C. Ewing, C.R.A. Catlow, T. Diaz De La Rubia, L.W. Hobbs, C. Kinoshita, H. Matzke, A.T. Motta, M. Natsai, E.K.H. Salje, E.R. Vance, S.J. Zinkle, J. Mater. Res. 13 (1998) 1434.
[9] F.G. Karioris, K. Appaji Gowda, L. Cartz, Radiat. Eff. Lett. 58 (1981) 1.
[10] A. Meldrum, L.A. Boatner, L.M. Wang, R.C. Ewing, Nucl. Instrum. and Meth. B 127 (1997) 160.
[11] P. Trocellier, Ann. Chim. Sci. Mater. 26 (2) (2001) 113.
[12] S. Soulet, J. Carpéna, J. Chaumont, O. Kaitasov, M.O. Ruault, J.C. Krupa, Nucl. Instrum. and Meth. B 184 (2001) 383.
[13] N. Clavier, N. Dacheux, P. Martinez, V. Brandel, R. Podor, P. Le Coustumer, J. Nucl. Mater. 335 (2004) 397.
[14] N. Dacheux, N. Clavier, G. Wallez, V. Brandel, J. Emery, M. Quarton, M. Genet, Mater Res. Bull. 40 (2005) 2225.
[15] G. Wallez, N. Clavier, N. Dacheux, M. Quarton, W. Van Beek, J. Solid State Chem. 179 (2006) 3007.
[16] N. Clavier, N. Dacheux, G. Wallez, M. Quarton, J. Nucl. Mater. 352 (2006) 209.
[17] N. Clavier, N. Dacheux, P. Martinez, E. du Fou de Kerdaniel, L. Aranda, R. Podor, Chem. Mater. 16 (2004) 3357.
[18] J.F. Ziegler, J.P. Biersack, U. Littmark, in: J.F. Ziegler (Ed.), The Stopping and Range of Ions in solids, vol. 1, Pergamon, New York, 1985.
[19] A. Meldrum, L.M. Wang, R.C. Ewing, Nucl. Instrum. and Meth. B 116 (1996) 220.
[20] J. Verstraete, L. Khouchaf, D. Bulteel, E. Garcia-Diaz, A.M. Flank, M.H. Tuilier, Cement Concr. Res. 34 (2004) 581.
[21] J.F. Gibbons, Proc. IEEE 60 (1972) 1062.
[22] C. Tamain, F. Garrido, L. Thomé, N. Dacheux, A. Özgümüs, A. Benyagoub, J. Nucl. Mater. 357 (2006) 206.
[23] C. Sabatier, Thesis, Université Paris-Sud-11, no. 7246, 2003.
[24] E. Pichot, N. Dacheux, J. Emery, J. Chaumont, V. Brandel, M. Genet, J. Nucl. Mater. 289 (2001) 219.
[25] A. Benyagoub, S. Klaumünzer, Radiat. Eff. Defect. Solids 126 (1993) 105.
[26] W.A. Johnson, P.A. Mehl, Trans. AIME 135 (1939) 416.
[27] M. Avrami, J. Chem. Phys. 7 (1939) 1103.
[28] C. Tamain, N. Dacheux, F. Garrido, A. Habert, N. Barré, A. Özgümüs, L. Thomé, J. Nucl. Mater. 358 (2006) 190.
[29] C. Tamain, N. Dacheux, F. Garrido, L. Thomé, J. Nucl. Mater. 362 (2007) 459.
[30] C. Tamain, A. Özgümüs, N. Dacheux, F. Garrido, L. Thomé, J. Nucl. Mater. 352 (2006) 217.